Cesium-Oleate Passivation for Stable Perovskite Photovoltaics

Xintong Guo,[†,‡] Teck Ming Koh,[†] Benny Febriansyah,[†,‡] Guifang Han,[†] Saikat Bhaumik,[†] Jia Li,[†] Nur Fadilah Jamaludin,[†,‡] Biplab Ghosh,[‡] Xiaodong Chen,[§] Subodh Mhaisalkar,[†,§] and Nripan Mathews,*[,†,§]

[†]Energy Research Institute @ NTU (ERI@N), Nanyang Technological University, Singapore 637553, Singapore.

[‡]Interdisciplinary Graduate School, Nanyang Technological University, Singapore 637371, Singapore.

[§]School of Materials Science and Engineering, Nanyang Technological University, 639798, Singapore.

ABSTRACT: Despite their emergence as promising materials for low-cost and efficient energy power generation technology, hybrid organic-inorganic lead-halide perovskites' instability towards moisture and heat stress remains a serious obstacle that needs to be tackled for commercialization. Here, we show improved moisture and thermal stability through the use of cesium oleate to modify the perovskite/hole transporting material (HTM) interface. Passivation using cesium oleate does not induce the formation of any low dimensional perovskites, suggesting that the organic species only passivates the perovskite's surface and grain boundaries. As a result, enhanced hydrophobic character of perovskite film is realized upon passivation, evidenced by high water contact angle of 107.4 degree and improved stability at ambient condition (relative humidity of ~70%, room temperature). Concomitantly, the proposed passivation strategy leads to increased amount of cesium concentration within the films, resulting in beneficial enhanced thermal stability of the film at 85°C. By maintaining the three-dimensional (3D) structure of the solar absorber while concurrently passivating the interfacial defects and vacancies, improved open-circuit voltage (V_{oc}) and unsacrificed short-circuit current density (J_{sc}) were obtained from the treated devices, leading to power conversion efficiencies of over 18%. When stored in a humid environment (relative humidity of ~55%), devices with cesium oleate passivation maintain 88% of its initial PCEs after 720 hours, degrading two times slower than those of the control. This work offers a strategy of coating 3D perovskites with unique combination of inorganic cation and long chain organics to provide hydrophobicity and moisture stability to the solar absorber layer, while maintaining good device performances.

KEYWORDS: *surface passivation, Cs-oleate, moisture stability, hydrophobicity, thermal stability*

INTRODUCTION

Over the last few years, perovskite solar cells (PSCs) have undergone a significant surge in efficiency, soaring from 3.8% in 2009 to over 24.2% in 2019.[1-3] Organic-inorganic lead-halide PSCs emerge from the confluence of many promising properties, including tunable direct band gap,[4-6] high optical absorption coefficient in visible range[7-8] and long carrier diffusion lengths.[9-11] Due to its solution-processability and Earth-abundant starting materials, PSCs are considered low-cost solar technology.[12-13] However, PSCs that have been developed are also notoriously unstable, especially over the long-term stability under ambient, atmospheric conditions.[14-16] This has been ascribed to partly the hydrophilicity of small organic cation as well as low formation energy of the three dimensional (3D) perovskites.[17-18] Thus, promoting the ambient stability of perovskites has become a key research focus.

Introducing relatively bulkier and more hydrophobic organic species on top of the perovskite layer is one of the primary solutions to address the material's intrinsic moisture instability.[19-23] However, such approach often involves the use of organics with ammonium functionality where common examples include butyl ammonium (BA^+),[19, 24] phenyl ethyl ammonium (PEA^+),[20, 25] 5-ammonium valeric acid (AVA),[26] and cyclohexyl methyl ammonium (CMA^+).[27] Although they were suggested to be capable of passivating the small cation vacancy within the 3D perovskite surface or grain boundaries, their presence also tends to induce formation of low dimensional perovskites due to the templating effect of the ammonium group.[28-29]

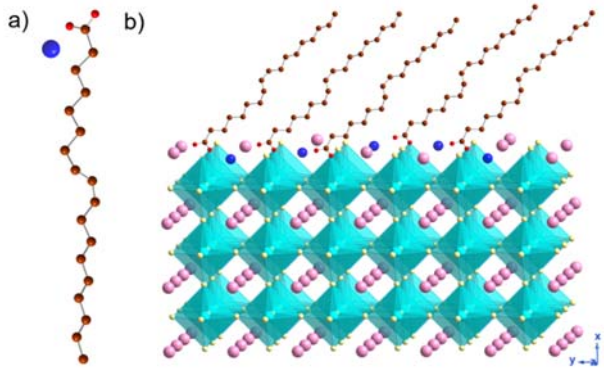

Figure 1. a.) Molecular structure of cesium oleate used to passivate perovskite film in this study. Blue, red, and brown spheres represent cesium, oxygen, and carbon atoms, respectively. b) Schematic showing how the organic long chain orientates outwardly to protect the perovskite layer. Pink spheres represent FA, MA or Cs cations; cyan and yellow ones represent Pb and halide atoms (I or Br) respectively.

As a consequence, since charge conduction in low dimensional perovskites is poorer, the power conversion efficiency of the overall PSCs often gets compromised, depending on the thickness of the low dimensional perovskite formed. In addition to ammonium-based organic cation, the accompanying anion has often been halides (bromide and iodide) that are light sensitive and prone towards oxidation.[19-21, 24-27] It has been reported that moisture induced degradation of perovskite can be catalysed by other factors such as light and oxygen due to degradation of different component of the materials, such as the halides.[30-31]

Motivated to improve the moisture tolerance of the PSCs, without sacrificing their power conversion efficiency, we aim to incorporate thin passivation layers that does not affect the perovskite's three-dimensional structure and does not contain any halide as the anion. To achieve this, we have selected cesium oleate (Cs-oleate),[32-35] comprising a long hydrocarbon organic endowed with carboxyl functionality (COO^-) and small inorganic cation (Cs^+) as our passivating agent (Figure 1a). The advantage of using the passivator is two-fold. First, by using Cs^+ as cation, low dimensional perovskite formation can be avoided. Instead, the Cs ion can diffuse into perovskite lattice and passivate the cuboctahedral vacancies of the host 3D perovskites due to its size and mobility. The presence of extra Cs^+ upon passivation is expected to improve the thermal stability of the material.[36-38] Secondly, the presence of carboxyl head in the oleate anion opens-up the possibility of it being anchored onto perovskite surface through chemical bonding with undercoordinated Pb^{2+} moiety. This allows the hydrophobic hydrocarbon chain to be arranged upwardly to protect perovskite film from moisture, slowing down the degradation of the material under ambient condition (Figure 1b). At the same time, the bonding with Pb^{2+} serves as passivation towards iodide vacancy, thus reducing the possible trap states within the material's surface and grain boundaries.

RESULTS AND DISCUSSION

Our perovskite films are based on the mixed-cation mixed-halide $Cs_{0.05}(MA_{0.17}FA_{0.83})_{0.95}Pb(I_{0.83}Br_{0.17})_3$ composition unless otherwise stated and were prepared as previously reported.[39] Meanwhile, the passivating agent Cs-oleate was synthesized based on a published procedure[35] with little modification and used freshly upon preparation (see SI). Toluene was employed as the solvent in our case instead of the more common 1-octadecene because the former has a much lower boiling point and thus would only require moderate temperature to remove solvent residue. The as prepared Cs-oleate was then spin coated on top of triple-cation perovskite, followed by an annealing process to form a hydrophobic layer on top of perovskite film. During the annealing process, color change of the films could be observed from blue to dark brown which becomes more obvious with higher concentration of the passivator (see Figure S1)

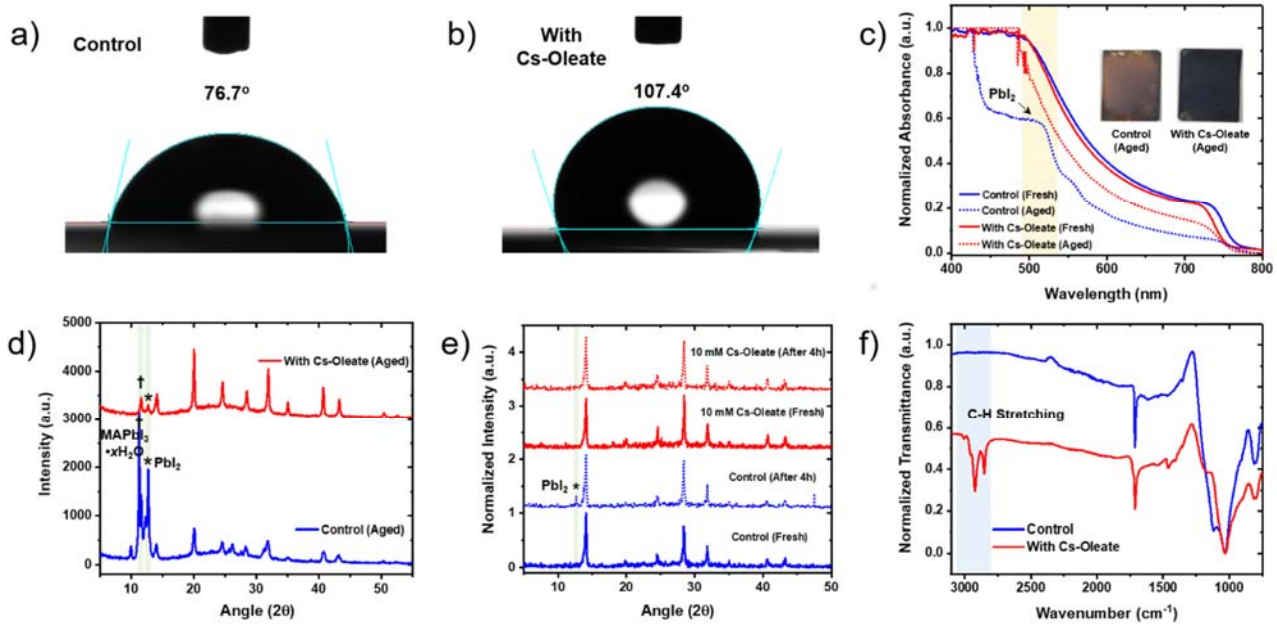

Figure 2. a) and b) Contact-angle measurement with water droplets for the pristine and Cs-oleate-passivated perovskite films, respectively. c) UV-visible light (UV-vis) absorption spectra of passivated and pristine films before and after exposure to ambient condition with relative humidity of ~70% at room temperature for 7 days. Green shaded region indicates the absorption of PbI_2 as a byproduct of perovskite degradation. Insets show photographs of aged perovskite films, demonstrating the enhanced moisture stability in the passivated perovskites. d) Associated glancing-angle X-ray diffraction (GAXRD) patterns of perovskite films before and after moisture exposure at the same condition as that of c). Consistently, severe degradation is observed in the pristine perovskite film. Asterisks and crosses denote the major reflections from hydrated perovskite and PbI_2,

respectively. e) GAXRD patterns of passivated and pristine films before and after heat-stress at 85 ºC for 4 hours under inert environment. f) Infrared spectra of the Cs-oleate-passivated and pristine perovskite films with blue shaded region indicates the C-H stretching of Cs-oleate passivator.

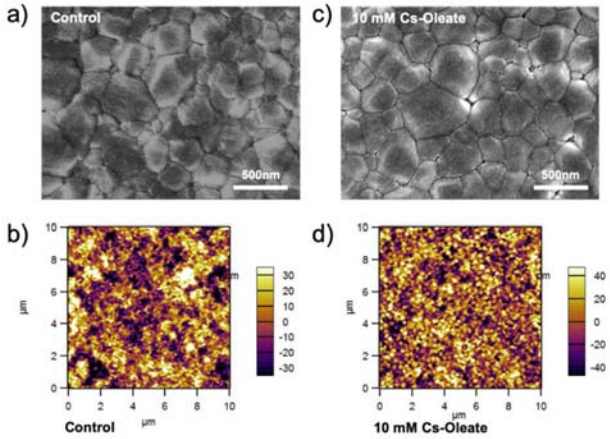

Figure 3. a) and c) Surface morphology image of the pristine perovskite film and treated with 10 mM Cs-oleate, respectively. b) and d) Associated topological view of the pristine and treated films.

With Cs-oleate passivation, surface property of perovskite films was observed to change significantly. In order to monitor the water repellancy, water contact angle measurement was conducted (Figures 2a and 2b).For the bare perovskite film, the contact angle is 76.7 degree while the contact angle of Cs-oleate passivated perovskite film was found to be significantly higher (107.4 degree), indicating a much higher hydrophobicity profile that could potentially slow down the degradation of perovskite by repelling moisture from attacking the perovskite surface.

Optical absorption of both pristine and passivated perovskite films before and after moisture exposure was recorded to monitor the stability of perovskite films (Figure 2c). The films were exposed to ambient condition with relative humidity of ~70% at room temperature for 7 days. It is clearly seen that over that period of time, the pristine perovskite film degrades much faster, evidenced by the diminishing visible light absorption of the 3D perovskite and concomitant increase of PbI_2 absorbance band at ~500 nm. Physically, while the bare perovskite film started to turn yellow, the passivated film did not show significant sign of degradation (Figure 2c, insets). Glancing-angle X-ray diffraction (GAXRD) patterns of perovskite films before and after moisture exposure affirm the results of UV-vis absorbance data where PbI_2 peak at 12.6º increases more significantly in the pristine film than in the passivated one (Figure 2d) during the testing period. In addition, the peak at 10.6º, believed to derive from perovskite hydrate intermediate, also shows much higher intensity in the control than the passivated film.[14] These results attest to the passivating effect of the Cs-oleate on enhancing the moisture stability of the perovskite at ambient condition.

Treating perovskite films with the passivator will concomitantly increase the cesium content in the materials. As shown in Figure 2e, we found that concentration of Cs-oleate as small as 10 mM is able to improve the thermal stability of perovskite film (Figure S2 shows the GAXRD patterns of thermal testing of films treated with different concentration of Cs-oleate). Heating the treated film at 85ºC for 4 hours under inert argon atmosphere in the absence of light, 3D perovskite was found to be intact, as evidenced by the GAXRD patterns of the aged samples. On the other hand, PbI_2 peak at 12.6º can clearly be seen in the control films under the same condition and period of testing. It has been reported that inorganic cesium cation plays a very crucial role in improving stability of perovskite towards thermal stress.[40-42] Thus, our method demonstrates a unique strategy of not only enhancing moisture resistance of 3D perovskite, but also thermal stability through cesium-doping.

To confirm the presence of Cs-oleate and its interaction with perovskite surface, we compared the Fourier-transform infrared spectroscopy (FTIR) spectrum of passivated perovskite film to that of bare perovskite film (Figure 2f). New peaks in the range of 2750 and 3100 cm^{-1} are ascribed to the C-H stretching bands in the organic oleate, and thus, it confirms the successful deposition of Cs-oleate on perovskite film after the spin coating process. The bonding between Cs-oleate and perovskite is assessed by measuring the FTIR peaks of Cs-oleate and PbI_2. Cs-oleate was deposited on top of PbI_2 film, and the FTIR spectrum is compared with the one of pristine Cs- oleate. We found that the C=O bond stretching in oleate is shifted from 1533 cm^{-1} to 1553 cm^{-1} (Figure S3a), indicating that the chemical environment of the atoms has changed. In particular, the shift to higher wavenumber is consistent with bond formation

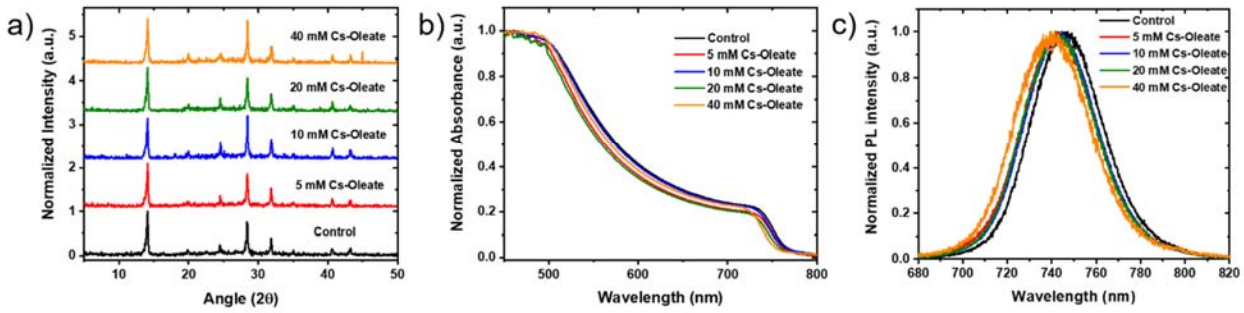

Figure 4. a) Glancing-angle X-ray diffraction (GAXRD) patterns, b) Ultra-violet (UV)-visible light absorption spectra, and c) Photoluminescence (PL) spectra.

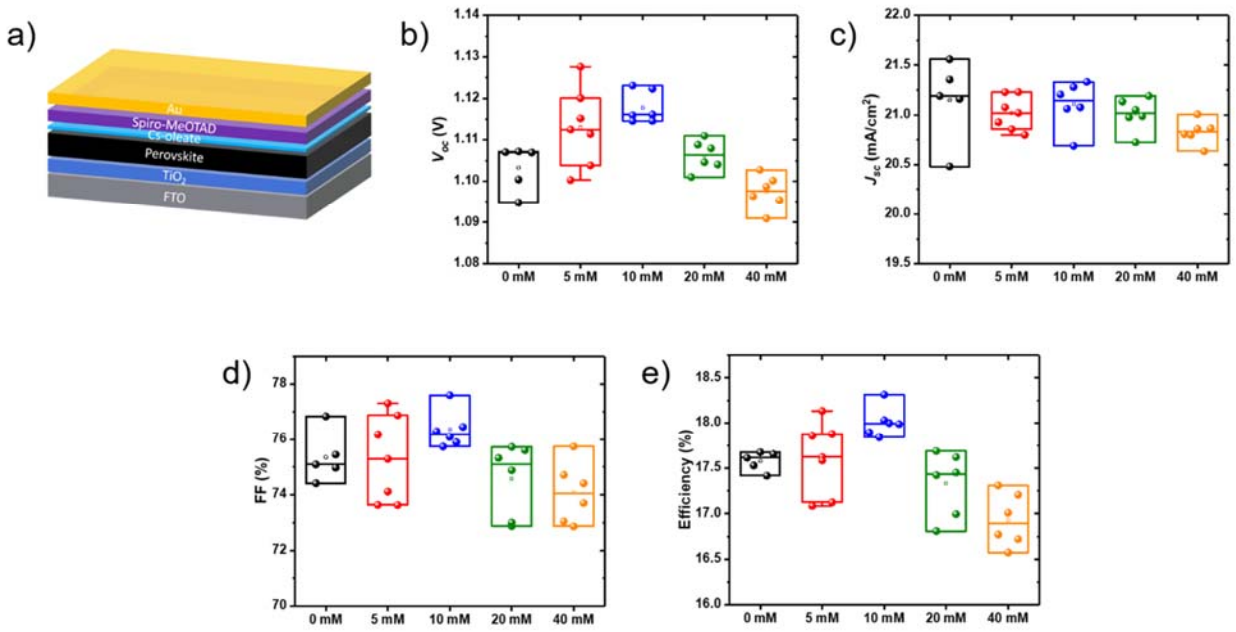

Figure 5. a) Perovskite solar cell architecture. Statistical representation of devices for the standard and Cs-oleate-treated devices for parameters (b) Open circuit voltage (V_{oc}), (c) Short-circuit current (J_{sc}), (d) Fill factor (FF), and (e) Power conversion efficiency.

between the oleate and Pb^{2+} atom where the bond resonance within carboxyl functionality becomes restricted, leading to stronger bond stretching (Figure S3b). Moreover, new peaks appear at 1323 cm^{-1} and 1441 cm^{-1}, which probably belong to Pb-oleate. We believe that similar bonding between Pb and oleate has also occurred during the passivation of perovskite films. Such bonding can then help anchor the organic oleate onto the perovskite surface with preferred orientation where the organic tails is facing outward, forming a hydrophobic net. Such hydrophobic layer believed to be responsible for protecting the perovskite film from moisture attachment as has been seen from previously mentioned investigations.

We carried-on probing the effect of different concentration of Cs-oleate towards perovskite films morphological, structural and optoelectronic properties. The surface morphology of pristine and passivated perovskite films is examined by Scanning Electron Microscopy (SEM) and Atomic Force Microscopy (AFM; Figure 3). As shown in Figures 3a, b and S4, the films treated with Cs-oleate feature compact uniform perovskite crystallites with grain sizes in the range of 200-400 nm, comparable if not better than the untreated film. This suggests that upon spin coating Cs-oleate solution, the 3D perovskite did not undergo reconstruction as no 2D perovskite was forming during annealing. The organic species instead only passivates the 3D perovskite's surface and grain boundaries rather than diffusing into its layer, as supported by the cross-sectional SEM images depicted in Figure S5. Cs-oleate treatment was also found to not significantly modify surface roughness of the 3D perovskite (Figures 3c, d, and S6). Concentrations of Cs-oleate of up to 10 mM still afford films with similar surface roughness to that of standard (25.3 nm of roughness in comparison to 20.5 nm), although a rougher film would be obtained at 40 mM concentration (30.3 nm), suggesting a thicker layer of passivator

could have formed at higher concentration. Table S1 summarizes the change of roughness of perovskite films as the function of Cs-oleate concentration.

Figure 4a shows the GAXRD profiles of perovskite films with different passivation concentration of Cs-oleate (0 mM, 5 mM, 10 mM, 20 mM and 40 mM). It is worth mentioning that no traces of low dimensional perovskite peaks were detected under XRD even with 40 mM concentration of Cs-oleate, affirming the notion that the oleate chain just passivates the surface and grain boundaries of 3D perovskite film, instead of diffusing and forming any low dimensional perovskite species. This demonstrates an advantage of utilizing oleate chain to passivate perovskite film as it keeps the perovskite 3D structure intact.

From the optical absorption spectra (Figure 4b), as the concentration of passivation increases, the absorption edges of perovskite films are found to be gradually blue-shifted. This suggests that the relative amount of Cs cations in the bulk perovskite films has increased after passivation using Cs-oleate. Due to its relatively smaller size, Cs^+ has no difficulties to diffuse into the perovskite lattice and this Cs-rich perovskite has larger bandgap compared with control triple cation perovskite, revealing the blue-shift in absorption edge.

The photoluminescence (PL) of perovskite films with and without Cs-oleate passivation were also examined and the spectra are depicted in Figure 4c. In agreement with their UV-vis absorption features, upon Cs-oleate passivation, the perovskite films emit PL peaks at lower wavelength compared with the pristine films.

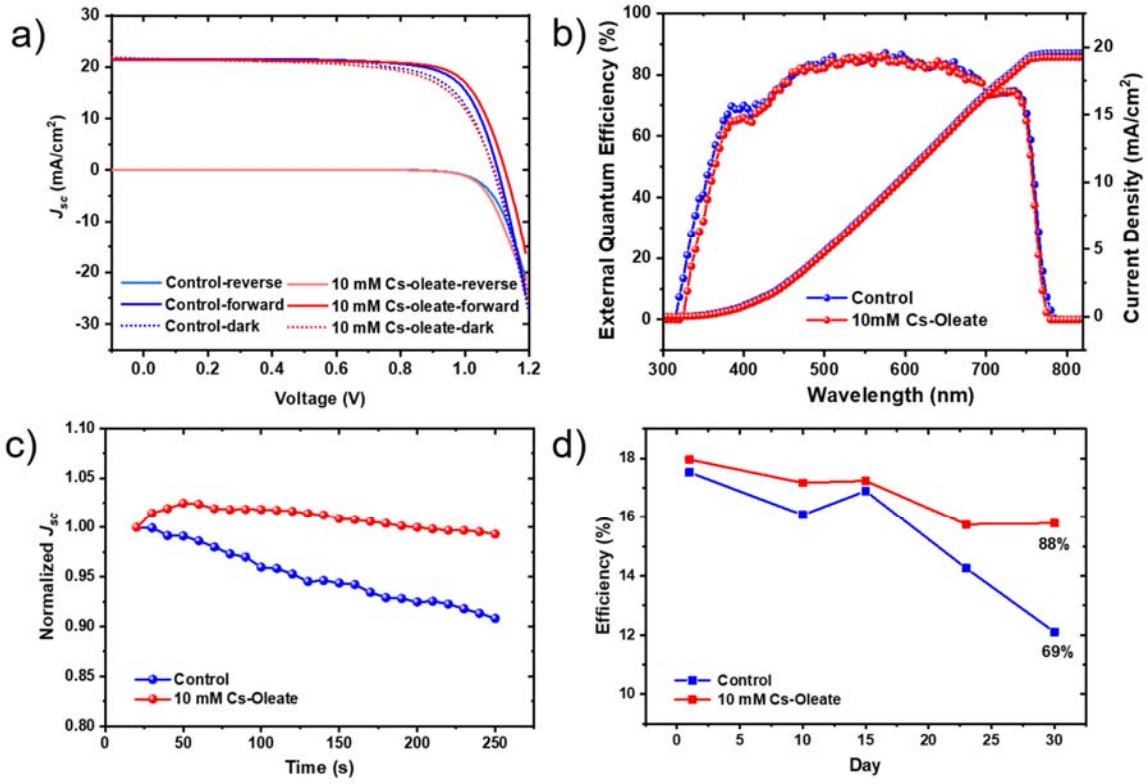

Figure 6. a) Current–voltage (J–V) curves of standard and 10 mM Cs-oleate-treated film devices subjected to forward and reverse bias scan direction. b) Incident photon to current conversion efficiency (IPCE) spectra and integrated current density of the standard and 10 mM Cs-oleate-treated film devices. c) Stabilized photocurrent density at the maximum power point (PPmax) vs time for the unsealed standard and 10 mM Cs-oleate-treated devices. d) Evaluation of photovoltaic power conversion efficiencies of unsealed mesoporous devices that were stored under ~55% relative humidity and dark conditions.

To assess whether the Cs-oleate-passivated perovskite films can enhance the solar cell performance, we fabricate devices based on an n type–intrinsic–p type (n–i–p) mesoporous heterojunction architecture (Figure 5a). Figure S5 shows the cross-sectional scanning electron microscopy (SEM) images of the solar cell devices prepared with standard triple-cation and Cs-oleate-treated perovskite films. The relative thickness of the perovskite layer for both devices was found to be similar at approximately 500 nm.

We studied the influence of passivation on open-circuit voltage (V_{oc}), short-circuit current density (J_{sc}), fill factor (FF) and power conversion efficiency (PCE) which are summarized in Figures 5b–5e. Cs-oleate passivated devices generally exhibit higher V_{oc} and FF, resulting in higher PCE as compared to standard devices. The gradual increase of V_{oc} as concentration of Cs-oleate increases up

to 10 mM is believed due to the increment in bandgap, as well as passivation effect towards surface defects of the perovskite layer that leads to reduced interfacial recombination. Interestingly, the J_{sc} of Cs-oleate-passivated devices are not greatly affected by the passivation up to 20 mM. We argue that this can be achieved due to the undisrupted structure of 3D perovskite upon passivation as no bulky organic cation is used. The charge transport is only compromised when the passivation is increased to 40 mM which is possibly due to the insulating nature of oleate chains that is lying in between the perovskite/spiro-OMeTAD interface.

The current-voltage (*I*-*V*) characteristics of best performing devices of Cs-oleate passivated (10 mM) and pristine perovskites measured under a simulated air mass (AM1.5) of 1 sun illumination (100 mW cm^{-2}) are depicted in Figure 6a. The device fabricated with a standard triple-cation perovskite yielded an average PCE of 17.58% with an average V_{oc}, J_{sc}, and FF of 1.10 V, 21.15 mA cm^{-2}, and 75.35%, respectively. The device fabricated with 10 mM modification gave an average PCE of 18.01% with a V_{oc} of 1.12 V, J_{sc} of 21.11 mA cm^{-2}, and FF of 76.34%. Consistent with the statistical data presented earlier, the passivated device exhibits better V_{oc} and FF, while retaining good J_{sc}. The relatively unchanged current collected from device upon Cs-oleate passivation is reflected in integrated current density from incident photon-to-current conversion efficiency (IPCE) spectra shown in Figure 6b where no major difference can be observed in comparison to that of control. The IPCE spectra of devices treated with other concentrations of Cs-oleate and their integrated current density can be found in Figure S7.

Additionally, we compared the reverse and forward scans of the best performance devices of control and 10 mM Cs-oleate-treated. The device fabricated with 10 mM Cs-oleate-treated films exhibited a V_{oc} of 1.12 V, J_{sc} of 21.33 mA cm^{-2}, FF of 76.44%, and PCE of 18.31%, observed in the reverse scan direction, and a V_{oc} of 1.09 V, J_{sc} of 21.64 mA cm^{-2}, FF of 66.67%, and PCE of 15.70% in the forward scan direction, whereas the standard device exhibited a V_{oc} of 1.10 V, J_{sc} of 21.56 mA cm^{-2}, FF of 74.41%, and PCE of 17.65% in the reverse scan direction and V_{oc} of 1.09 V, J_{sc} of 21.64 mA cm^{-2}, FF of 69.53%, and PCE of 16.34% in the forward scan direction under 1 sun illumination. The reverse scan shows enhanced V_{oc}, FF, and PCE when compared to forward scan for 10 mM Cs-oleate-treated and standard devices.

Figure 6c shows the stabilized photocurrent density measured as a function of time to compare the performance of Cs-oleate passivated device and the control device. It was found that device passivated with Cs-oleate displays better stability towards long-term light soaking as compared to control device. To demonstrate the benefit of having Cs-oleate as the perovskite capping layer toward moisture, we carried out shelf stability studies of complete devices based on 10 mM and compare it with the standard under ambient environments at room temperature under relative humidity (RH) of ~55% without any encapsulation. The Cs-oleate passivated device retained 88% of its original power conversion efficiency after 720 hours while that of control device was dropped to ~69%, which is unsatisfied for practical working condition (Figure 6d). Therefore, the Cs-oleate significantly improved the moisture and thermal stabilities of perovskite solar cells in agreement with improved stability features of perovskite films discussed prior.

CONCLUSION

In summary, efficient and moisture-stable perovskite solar cells are fabricated by passivating the perovskite film with a layer of Cs-oleate. The Cs cation filled the vacancies of organic cations on perovskite surface and grain boundaries, while the carboxyl group in oleate anchored the organic chain to Pb-X framework, significantly improving the moisture tolerance of perovskite. The water contact angle increased from 76.7 degree to 107.4 degree, indicating that the surface property changed from hydrophilic to hydrophobic. For the device performance, Voc and fill factor improved with Cs-oleate treatment due to the passivation of defects. The overall efficiency also increased with smaller deviation compared to the control devices. Device efficiency of passivated device retained close to 90% of its initial PCE over 720 hours under 55% RH at room temperature. Therefore, surface passivation using Cs-oleate is a feasible way to improve the moisture stability of perovskite solar cells with improved performance.

ASSOCIATED CONTENT

Materials synthesis, experimental procedures, and additional spectra (pdf). The Supporting Information is available free of charge on the ACS Publications website.

AUTHOR INFORMATION

Corresponding Author

*Email: nripan@ntu.edu.sg.

Notes

The authors declare no competing financial interest.

ACKNOWLEDGMENT

The authors would like to acknowledge the funding from the Singapore National Research Foundation through the Singapore–Berkeley Research Initiative for Sustainable Energy (SinBeRISE) CREATE Program, Office of Naval Research Global (ONRG-NICOP-N62909-17-1-2155), Intra-CREATE Collaborative Grant (NRF2018-ITC001-001) and the Competitive Research Program: NRF–CRP14–2014–03. X.T. Guo would like to thank Mr. K. Thirumal for his kind help in PESA measurement.

REFERENCES

(1) Kojima, A.; Teshima, K.; Shirai, Y.; Miyasaka, T., Organometal Halide Perovskites as Visible-Light Sensitizers for Photovoltaic Cells, *J. Am. Chem. Soc.* **2009**, *131* (17), 6050-6051.

(2) Best Research-Cell Efficiencies Rev. 16-04-2019 (NREL, 2019); https://www.nrel.gov/pv/assets/pdfs/best-research-cell-efficiencies-190416.pdf.

(3) Gratzel, M., The light and shade of perovskite solar cells. *Nat. Mater.* **2014,** *13* (9), 838-842.

(4) Pellet, N.; Gao, P.; Gregori, G.; Yang, T. Y.; Nazeeruddin, M. K.; Maier, J.; Gratzel, M., Mixed-organic-cation perovskite photovoltaics for enhanced solar-light harvesting. *Angew. Chem. Int. Ed.* **2014,** *53* (12), 3151-3157.

(5) Noh, J. H.; Im, S. H.; Heo, J. H.; Mandal, T. N.; Seok, S. I., Chemical management for colorful, efficient, and stable inorganic-organic hybrid nanostructured solar cells. *Nano Lett.* **2013,** *13* (4), 1764-1769.

(6) McMeekin, D. P.; Sadoughi, G.; Rehman, W.; Eperon, G. E.; Saliba, M.; Hörantner, M. T.; Haghighirad, A.; Sakai, N.; Korte, L.; Rech, B.; Johnston, M. B.; Herz, L. M.; Snaith, H. J., A mixed-cation lead mixed-halide perovskite absorber for tandem solar cells. *Science* **2016**, *351*, 152-155.

(7) Yang,W. S.; Noh, J. H.; Jeon, N. J.; Kim, Y. C.; Ryu, S.; Seo, J.; Seok, S. L., High-performance photovoltaic perovskite layers fabricated through intramolecular exchange. *Science* **2015**, *348*, 1234-1237.

(8) Hao, F.; Stoumpos, C. C.; Cao, D. H.; Chang, R. P. H.; Kanatzidis, M. G., Lead-free solid-state organic–inorganic halide perovskite solar cells. *Nat. Photonics* **2014,** *8* (6), 489-494.

(9) Xing, G.; Mathews, N.; Sun, S.; Lim, S. S.; Lam, Y. M.; Grätzel, M.; Mhaisalkar, S.; Sum, T. C., Long-Range Balanced Electron- and Hole-Transport Lengths in Organic-Inorganic $CH_3NH_3PbI_3$. *Science* **2013**, *342*, 344-347.

(10) Shi, D.; Adinolfi, V.; Comin, R.; Yuan, M.; Alarousu, E.; Buin, A.; Chen, Y.; Hoogland, S.; Rothenberger, A.; Katsiev, K.; Losovyj, Y.; Zhang, X.; Dowben, P. A.; Mohammed, O. F.; Sargent, E. H.; Bakr, O. M., Low trap-state density and long carrier diffusion in organolead trihalide perovskite single crystals. *Science* **2015**, *347*, 519-522.

(11) Stranks, S. D.; Eperon, G. E.; Grancini, G.; Menelaou, C.; Alcocer, M. J. P.; Leijtens, T.; Herz, L. M.; Petrozza, A.; Snaith, H. J., Electron-Hole Diffusion Lengths Exceeding 1 Micrometer in an Organometal Trihalide Perovskite Absorber. *Science* **2013**, *342*, 341-344.

(12) Mei, A.; Li, X.; Liu, L.; Ku, Z.; Liu, T.; Rong, Y.; Xu, M.; Hu, M.; Chen, J.; Yang, Y.; Grätzel, M.; Han, H., A hole-conductor–free, fully printable mesoscopic perovskite solar cell with high stability. *Science* **2014**, *345*, 295-298.

(13) Fu, F.; Feurer, T.; Jager, T.; Avancini, E.; Bissig, B.; Yoon, S.; Buecheler, S.; Tiwari, A. N., Low-temperature-processed efficient semi-transparent planar perovskite solar cells for bifacial and tandem applications. *Nat. Commun.* **2015,** *6*, 8932.

(14) Leguy, A. M. A.; Hu, Y.; Campoy-Quiles, M.; Alonso, M. I.; Weber, O. J.; Azarhoosh, P.; van Schilfgaarde, M.; Weller, M. T.; Bein, T.; Nelson, J.; Docampo, P.; Barnes, P. R. F., Reversible Hydration of CH3NH3PbI3 in Films, Single Crystals, and Solar Cells. *Chem. Mater.* **2015,** *27* (9), 3397-3407.

(15) Aristidou, N.; Sanchez-Molina, I.; Chotchuangchutchaval, T.; Brown, M.; Martinez, L.; Rath, T.; Haque, S. A., The Role of Oxygen in the Degradation of Methylammonium Lead Trihalide Perovskite Photoactive Layers. *Angew. Chem. Int. Ed. Engl.* **2015,** *54* (28), 8208-8212.

(16) Conings, B.; Drijkoningen, J.; Gauquelin, N.; Babayigit, A.; D'Haen, J.; D'Olieslaeger, L.; Ethirajan, A.; Verbeeck, J.; Manca, J.; Mosconi, E.; Angelis, F. D.; Boyen, H.-G., Intrinsic Thermal Instability of Methylammonium Lead Trihalide Perovskite. *Adv. Energy Mater.* **2015,** *5* (15), 1500477.

(17) Quan, L. N.; Yuan, M.; Comin, R.; Voznyy, O.; Beauregard, E. M.; Hoogland, S.; Buin, A.; Kirmani, A. R.; Zhao, K.; Amassian, A.; Kim, D. H.; Sargent, E. H., Ligand-Stabilized Reduced-Dimensionality Perovskites. *J. Am. Chem. Soc.* **2016,** *138* (8), 2649-2655.

(18) Tsai, H.; Nie, W.; Blancon, J.-C.; Stoumpos, C. C.; Asadpour, R.; Harutyunyan, B.; Neukirch, A. J.; Verduzco, R.; Crochet, J. J.; Tretiak, S.; Pedesseau, L.; Even, J.; Alam, M. A.; Gupta, G.; Lou, J.; Ajayan, P. M.; Bedzyk, M. J.; Kanatzidis, M. G.; Mohite, A. D., High-efficiency two-dimensional Ruddlesden–Popper perovskite solar cells. *Nature* **2016,** *536* (7616), 312-316.

(19) Koh, T. M.; Shanmugam, V.; Guo, X.; Lim, S. S.; Filonik, O.; Herzig, E. M.; Müller-Buschbaum, P.; Swamy, V.; Chien, S. T.; Mhaisalkar, S. G.; Mathews, N., Enhancing moisture tolerance in efficient hybrid 3D/2D perovskite photovoltaics. *J. Mater. Chem. A* **2018,** *6* (5), 2122-2128.

(20) Wang, F.; Geng, W.; Zhou, Y.; Fang, H.-H.; Tong, C.-J.; Loi, M. A.; Liu, L.-M.; Zhao, N., Phenylalkylamine Passivation of Organolead Halide Perovskites Enabling High-Efficiency and Air-Stable Photovoltaic Cells. *Adv. Mater.* **2016,** *28* (45), 9986-9992.

(21) Salim, K. M. M.; Koh, T. M.; Bahulayan, D.; Harikesh, P. C.; Jamaludin, N. F.; Febriansyah, B.; Bruno, A.; Mhaisalkar, S.; Mathews, N., Extended Absorption Window and Improved Stability of Cesium-Based Triple-Cation Perovskite Solar Cells Passivated with Perfluorinated Organics. *ACS Energy Lett.* **2018,** *3* (5), 1068-1076.

(22) Niu, T.; Lu, J.; Tang, M.-C.; Barrit, D.; Smilgies, D.-M.; Yang, Z.; Li, J.; Fan, Y.; Luo, T.; McCulloch, I.; Amassian, A.; Liu, S.; Zhao, K., High performance ambient-air-stable $FAPbI_3$ perovskite solar cells with molecule-passivated Ruddlesden–Popper/3D heterostructured film. *Energy & Environ. Sci.* **2018,** *11* (12), 3358-3366.

(23) Zhang, Y.; Wang, P.; Tang, M. C.; Barrit, D.; Ke, W.; Liu, J.; Luo, T.; Liu, Y.; Niu, T.; Smilgies, D. M.; Yang, Z.; Liu, Z.; Jin, S.; Kanatzidis, M. G.; Amassian, A.; Liu, S. F.; Zhao, K., Dynamical Transformation of Two-Dimensional Perovskites with Alternating Cations in the Interlayer Space for High-Performance Photovoltaics. *J. Am. Chem. Soc.* **2019,** *141* (6), 2684-2694.

(24) Lin, Y.; Bai, Y.; Fang, Y.; Chen, Z.; Yang, S.; Zheng, X.; Tang, S.; Liu, Y.; Zhao, J.; Huang, J., Enhanced Thermal Stability in Perovskite Solar Cells by Assembling 2D/3D Stacking Structures. *J. Phys. Chem. Lett.* **2018,** *9* (3), 654-658.

(25) Hu, Y.; Schlipf, J.; Wussler, M.; Petrus, M. L.; Jaegermann, W.; Bein, T.; Muller-Buschbaum, P.; Docampo, P., Hybrid Perovskite/Perovskite Heterojunction Solar Cells. *ACS Nano* **2016,** *10* (6), 5999-6007.

(26) Ye, T.; Bruno, A.; Han, G.; Koh, T. M.; Li, J.; Jamaludin, N. F.; Soci, C.; Mhaisalkar, S. G.; Leong, W. L., Efficient and Ambient-Air-Stable Solar Cell with Highly Oriented 2D@3D Perovskites. *Adv. Funct. Mater.* **2018,** *28* (30), 1801654.

(27) Ma, C.; Leng, C.; Ji, Y.; Wei, X.; Sun, K.; Tang, L.; Yang, J.; Luo, W.; Li, C.; Deng, Y.; Feng, S.; Shen, J.; Lu, S.; Du, C.; Shi, H., 2D/3D perovskite hybrids as moisture-tolerant and efficient light absorbers for solar cells. *Nanoscale* **2016,** *8* (43), 18309-18314.

(28) Koh, T. M.; Thirumal, K.; Soo, H. S.; Mathews, N., Multidimensional Perovskites: A Mixed Cation Approach Towards Ambient Stable and Tunable Perovskite Photovoltaics. *ChemSusChem* **2016,** *9* (18), 2541-2558.

(29) Saidaminov, M. I.; Mohammed, O. F.; Bakr, O. M., Low-Dimensional-Networked Metal Halide Perovskites: The Next Big Thing. *ACS Energy Lett.* **2017,** *2* (4), 889-896.

(30) Wang, S.; Jiang, Y.; Juarez-Perez, E. J.; Ono, L. K.; Qi, Y., Accelerated degradation of methylammonium lead iodide perovskites induced by exposure to iodine vapour. *Nat. Energy* **2016,** *2* (1), 16195.

(31) Wang, L.; Zhou, H.; Hu, J.; Huang, B.; Sun, M.; Dong, B.; Zheng, G.; Huang, Y.; Chen, Y.; Li, L.; Xu, Z.; Li, N.; Liu, Z.; Chen, Q.; Sun, L-D.; Yan, C-H., A Eu^{3+}-Eu^{2+} ion redox shuttle imparts operational durability to Pb-I perovskite solar cells. *Science* **2019**, *363*, 265-270.

(32) Almeida, G.; Goldoni, L.; Akkerman, Q.; Dang, Z.; Khan, A. H.; Marras, S.; Moreels, I.; Manna, L., Role of Acid-Base Equilibria in the Size, Shape, and Phase Control of Cesium Lead Bromide Nanocrystals. *ACS Nano* **2018,** *12* (2), 1704-1711.

(33) Pan, J.; Sarmah, S. P.; Murali, B.; Dursun, I.; Peng, W.; Parida, M. R.; Liu, J.; Sinatra, L.; Alyami, N.; Zhao, C.; Alarousu, E.; Ng, T. K.; Ooi, B. S.; Bakr, O. M.; Mohammed, O. F., Air-Stable Surface-Passivated Perovskite Quantum Dots for Ultra-Robust, Single- and Two-Photon-Induced Amplified Spontaneous Emission. *J. Phys. Chem. Lett.* **2015,** *6* (24), 5027-33.

(34) Yassitepe, E.; Yang, Z.; Voznyy, O.; Kim, Y.; Walters, G.; Castañeda, J. A.; Kanjanaboos, P.; Yuan, M.; Gong, X.; Fan, F.; Pan, J.; Hoogland, S.; Comin, R.; Bakr, O. M.; Padilha, L. A.; Nogueira, A. F.; Sargent, E. H., Amine-Free Synthesis of Cesium Lead Halide Perovskite Quantum Dots for Efficient Light-Emitting Diodes. *Adv. Func. Mater.* **2016,** *26* (47), 8757-8763.

(35) Protesescu, L.; Yakunin, S.; Bodnarchuk, M. I.; Krieg, F.; Caputo, R.; Hendon, C. H.; Yang, R. X.; Walsh, A.; Kovalenko, M. V., Nanocrystals of Cesium Lead Halide Perovskites (CsPbX(3), X = Cl, Br, and I): Novel Optoelectronic Materials Showing Bright Emission with Wide Color Gamut. *Nano Lett.* **2015,** *15* (6), 3692-6.

(36) Chen, H.; Xiang, S.; Li, W.; Liu, H.; Zhu, L.; Yang, S., Inorganic Perovskite Solar Cells: A Rapidly Growing Field. *Solar RRL* **2018,** *2* (2).

(37) Liang, J.; Wang, C.; Wang, Y.; Xu, Z.; Lu, Z.; Ma, Y.; Zhu, H.; Hu, Y.; Xiao, C.; Yi, X.; Zhu, G.; Lv, H.; Ma, L.; Chen, T.; Tie, Z.; Jin, Z.; Liu, J., All-Inorganic Perovskite Solar Cells. *J. Am. Chem. Soc.* **2016,** *138* (49), 15829-15832.

(38) Wang, K.; Jin, Z.; Liang, L.; Bian, H.; Bai, D.; Wang, H.; Zhang, J.; Wang, Q.; Liu, S., All-inorganic cesium lead iodide perovskite solar cells with stabilized efficiency beyond 15. *Nat. Commun.* **2018,** *9* (1), 4544.

(39) Saliba, M.; Matsui, T.; Seo, J. Y.; Domanski, K.; Correa-Baena, J. P.; Nazeeruddin, M. K.; Zakeeruddin, S. M.; Tress, W.; Abate, A.; Hagfeldt, A.; Gratzel, M., Cesium-containing triple cation perovskite solar cells: improved stability, reproducibility and high efficiency. *Energy Environ. Sci.* **2016,** *9* (6), 1989-1997.

(40) Sutton, R. J.; Eperon, G. E.; Miranda, L.; Parrott, E. S.; Kamino, B. A.; Patel, J. B.; Hörantner, M. T.; Johnston, M. B.; Haghighirad, A. A.; Moore, D. T.; Snaith, H. J., Bandgap-Tunable Cesium Lead Halide Perovskites with High Thermal Stability for Efficient Solar Cells. *Adv. Energy Mater.* **2016,** *6* (8), 1502458.

(41) Niu, G.; Li, W.; Li, J.; Liang, X.; Wang, L., Enhancement of thermal stability for perovskite solar cells through cesium doping. *RSC Adv.* **2017,** *7* (28), 17473-17479.

(42) Bella, F.; Renzi, P.; Cavallo, C.; Gerbaldi, C., Caesium for Perovskite Solar Cells: An Overview. *Chemistry* **2018,** *24* (47), 12183-12205.

Supporting Information

Cesium-Oleate Passivation for Stable Perovskite Photovoltaics

Xintong Guo,[†,‡] Teck Ming Koh,[†] Benny Febriansyah,[†,‡] Guifang Han,[†] Saikat Bhaumik,[†] Jia Li,[†] Nur Fadilah Jamaludin,[†,‡] Biplab Ghosh,[‡] Xiaodong Chen,[§] Subodh Mhaisalkar,[†,§] and Nripan Mathews,*[,†,§]

[†]Energy Research Institute @ NTU (ERI@N), Nanyang Technological University, Singapore 637553, Singapore.

[‡]Interdisciplinary Graduate School, Nanyang Technological University, Singapore 637371, Singapore.

[§]School of Materials Science and Engineering, Nanyang Technological University, 639798, Singapore.

Materials synthesis.

Chemicals.

Cesium-oleate was prepared by mixing cesium carbonate (Cs_2CO_3), oleic acid (molar ratio 1:3) and anhydrous toluene in a round bottom flask. The mixture were stirred and heated in 100ºC-oil bath until the Cs_2CO_3 was fully dissolved. Measure the volume of the solution to calculate the concentration of Cs-oleate in toluene. Dilute Cs-oleate solution into 5 mM, 10 mM, 20 mM, and 40 mM with anhydrous toluene in glovebox.

Methyammonium bromide (MABr), formamidinium iodide (FAI), and cesium iodide (CsI) were purchased from Sigma Adrich. Lead bromide ($PbBr_2$) and lead iodide (PbI_2) were from purchased from TCI Chemicals.

Thin film and Solar cell fabrication.

Pre-etched FTO substrates (NSG TEC™ 15), with the size of 2.1 cm x 1.7 cm, were ultrasonic cleaned in detergent, DI water and ethanol consequently for 30 min each. After dried with nitrogen gas, the substrates surfaces were treated in UV ozone for 15 min before spin coating.

The precursor for TiO_2 compact layer was prepared by mixing tetrabutyltitanate, anhydrous ethanol, diethanolamine and DI water (weight ratio 227:890:28:70). The mixture were stirred for 24 hours, followed by standing for 24 hours. Then the compact TiO_2 layer was prepared by spin coating the precursor on FTO substrates at 5000 rpm and heat treatment at 500 ºC for 2 hours. After cooling to room temperature, the substrates were treated in 20 mM $TiCl_4$ solution for 30 min in oven at 70 ºC, followed by the annealing at 500 ºC for 30 min. TiO_2 paste (DYESOL-30NRD) was diluted in ethanol (1:7 w/w) and kept stirring for 3 hours. Then the solution was spin-coated onto the blocking layer to form a mesoporous TiO_2 layer. $TiCl_4$ treatment was done to the substrates using 20 mM $TiCl_4$ solution at 70 ºC for 30 min. Followed by annealing at 500 ºC for 30 min before spin coating perovskite films.

Perovskite solution (1.35 M) was prepared by dissolving CsI, MABr, FAI, $PbBr_2$ and PbI_2 crystals (0.05:0.17:0.83:0.17:0.83) in DMSO/DMF mix solvent (volume ratio 1:4). Perovskite solution was dropped onto prepared substrates and spin coated at 6000 rpm for 30 sec. During spin coating, anti-solvent of chlorobenzene was dipped onto spinning sample to form smooth films, followed by an annealing pro-

cess at 100 ºC for 60 min. After cooling down to room temperature, Cs-oleate solution of different concentration are deposited onto perovskite film at 4000 rpm for 30 s, while the control sample was coated with bare toluene solvent. After the deposition of Cs-oleate or bare toluene solvent, all the samples were annealed at 100 ºC for 15 min. Samples were cooled down to room temperature and a 70 mg/ml Spiro-OMeTAD (in chlorobenzene) solution was spin coated on perovskite film at 5000 rpm for 30 sec. Au electrodes (~100 nm) were thermal evaporated on samples with the size of 0.2 cm x 0.2 cm.

Instrumentation and Methods

UV-Vis spectroscopy, steady-state photoluminescence (SSPL) spectroscopy, field- emission scanning electron microscopy (FE-SEM), and atomic force miscroscopy (AFM). UV-vis absorption and SSPL spectra were recorded using a SHIMADZU UV-3600 spectrophotometer, with an integrating sphere (ISR-3100) in the wavelength range 300-800nm, and Horiba Fluoromax-3 spectrometer, with 0.5nm wavelength resolution, respectively. Surface morphology and cross-section images of the 2D perovskite thin films and solar cell devices were recorded using a JEOL JSM-7600F field emission scanning electron microscope (FESEM), with an accelerating voltage of 5kV. AFM measurements were conducted using a Bruker Icon microscope. All measurements were performed in the standard tapping mode with OTESPA-R3 tips from Bruker.

Time-Resolved Photoluminescence (PL) spectroscopy. The micro-PL setup used is based on a fibre-coupled microscope system. The excitation path and emission collection come from a VIS-NIR microscope objective (10x, NA= 0.65). Samples were excited with a 40-MHz-repetition-rate, picosecond-pulse light sources at 405 nm (Picoquant P-C-405B) light-emitting diode, and the spot size was about 10 μm. The time-resolved emitted signal was collected through a fibre-coupled Acton monochromator (SpectraPro 2300), to filter the desired wavelength, and detected by Micro Photon Devices single-photon avalanche photodiode (LDH-P-670). The signal was then acquired by a time-correlated single photon counting card (Pico Harp TSCPC module and Picosecond Event Timer 300). Temporal resolution is ~50 ps.

Infra-red (IR) spectroscopy. IR spectra of the samples were measured in transmission mode using a VERTEX 80V FT-IR Spectrophotometer with an ATR (attenuated total reflectance) accessory and a

scanning resolution of 4 cm-1s-1. The measurement was carried out under vacuum to minimize the effect of atmospheric particles of the surroundings.

Glancing angle X-ray diffraction. Glancing-angle X-ray diffraction measurements were conducted using a Bruker AXS D8 ADVANCE system with Cu Ka radiation (l = 1.5418Å). The XRD spectra were recorded with an incident angle of 5°, a step size of 0.05°, and a delay time of 1s for each step.

Solar cell devices and incident photon-to-current efficiencies. Photovoltaic characteristics of the solar cell devices were measured in the reverse scanning direction (from V_{oc} to J_{sc}), with a sweep rate of 100 mV s^{-1}, under AM1.5G (100mW.cm^{-2}) spectral irradiation from a solar simulator (Newport 91190A) incorporating a 450W xenon lamp (model 81172, Oriel) calibrated with a Si reference cell (Oriel PN91150). Devices were characterized through a 0.09cm^2 black mask. Incident photon-to-current efficiency (IPCE) was measured using a photovoltaic quantum efficiency (QE) instrument, PVE300 (Bentham), with a dual xenon/quartz halogen light source, measured in DC mode, and no bias light was used in the wavelength range 300 – 800nm. A Coherent OPerA Solo optical parametric amplifier pumped with a Coherent Libra^{TM} regenerative amplifier (50fs, 1kHz, 800nm) was used to generate a 600 nm excitation beam.

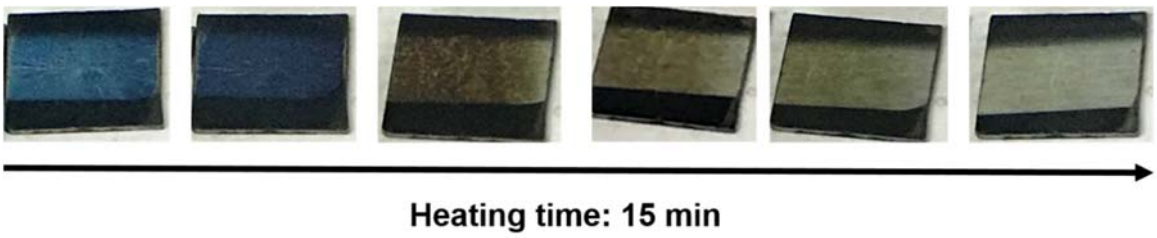

Figure S1. Photographs of a perovskite film treated with Cs-oleate (40mM in this case). Color change was observed during the annealing process applied upon spin coating, implying the reaction happening between Cs-oleate and perovskite films.

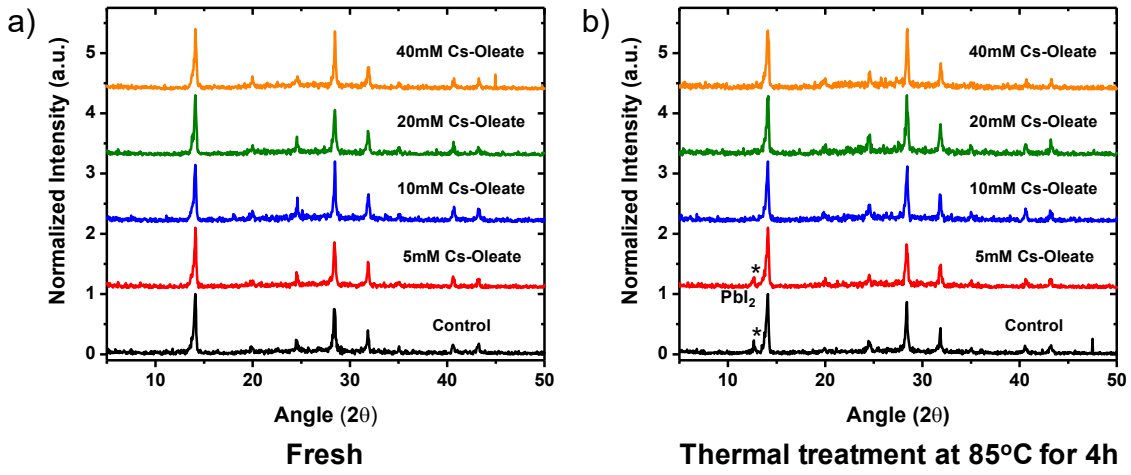

Figure S2. Glancing-angle X-ray diffraction (GAXRD) patterns of pristine and Cs-oleate treated perovskite films before (a) and after (b) exposure to thermal stress at 85°C for 4 hours under inert atmosphere environment. Asterix denote peak of PbI_2 produced upon degradation of the perovskite.

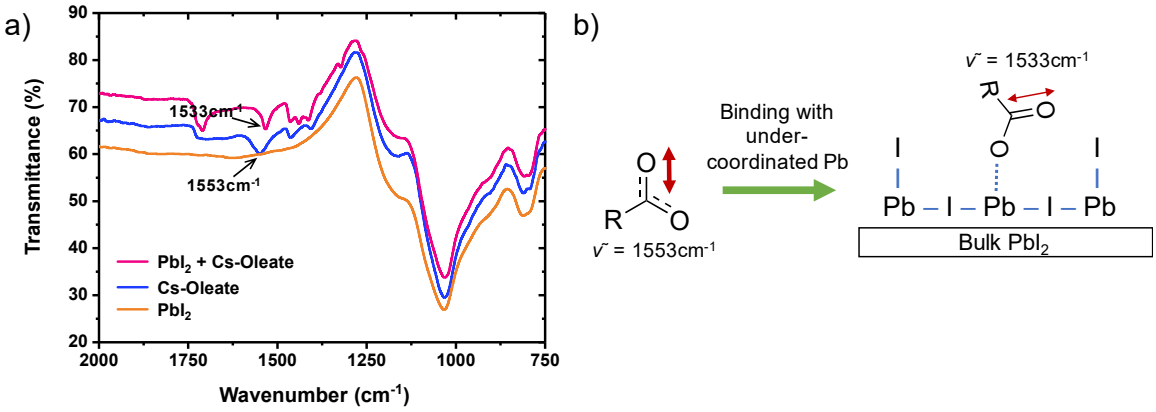

Figure S3. a) Infra-red (IR) spectra of PbI_2, Cs-oleate and Cs-oleate-treated PbI_2. There is a shift in $1553cm^{-1}$ peak to around $1533cm^{-1}$ which is believed due to binding of the carboxylate group with the under-coordinated Pb in PbI_2. The coordination causes the C=O binding to weaken, thus leads to stretching shift to lower wavenumber as schematically shown in Figure b). Green shaded region shows new peaks in Cs-oleate-treated PbI_2 that appear at $1323cm^{-1}$ and $1441cm^{-1}$.

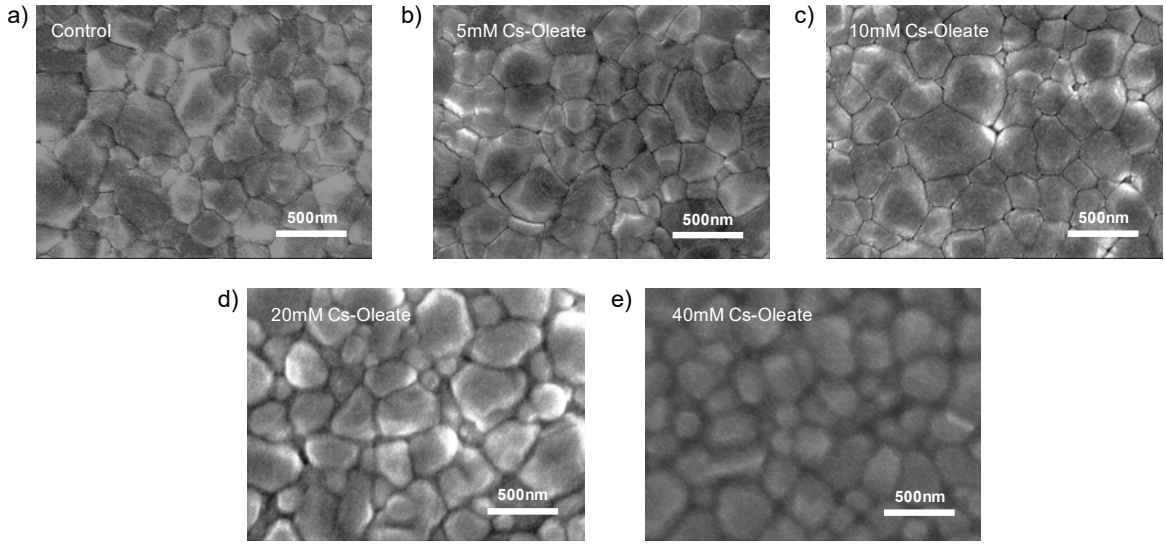

Figure S4. Top morphological view of field electric scanning electron microscope (FE-SEM) images of 3D perovskites without and with Cs-oleate treatment. a) for control, while b) -e) for 5 mM, 10 mM, 20 mM, and 40 mM Cs-oleate-treated films respectively.

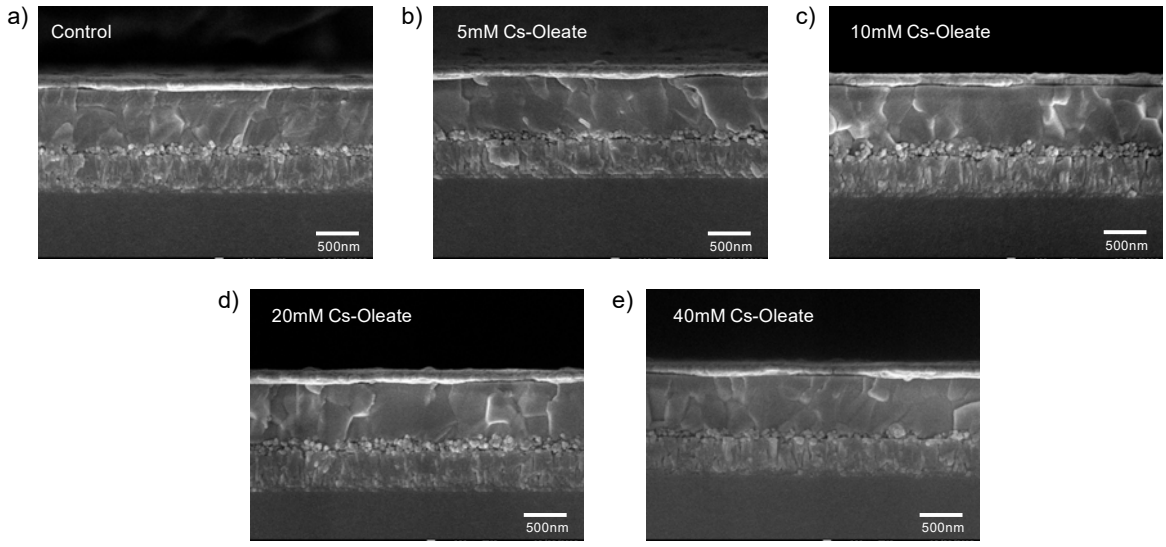

Figure S5. Cross-sectional view of field electric scanning electron microscope (FE-SEM) images of perovskite solar cells without and with Cs-oleate treatment. a) for control, while b) -e) for 5 mM, 10 mM, 20 mM, and 40 mM Cs-oleate-treated devices respectively. The device architecture is shown in Figure 5a where mesoporous titanium dioxide (TiO_2) and organic Spiro-MeOTAD are used as electron- and hole-transporting materials, respectively. As can be seen, treatment with Cs-oleate with concentration as high as 40mM does not cause restructuring of perovskite crystallite grains.

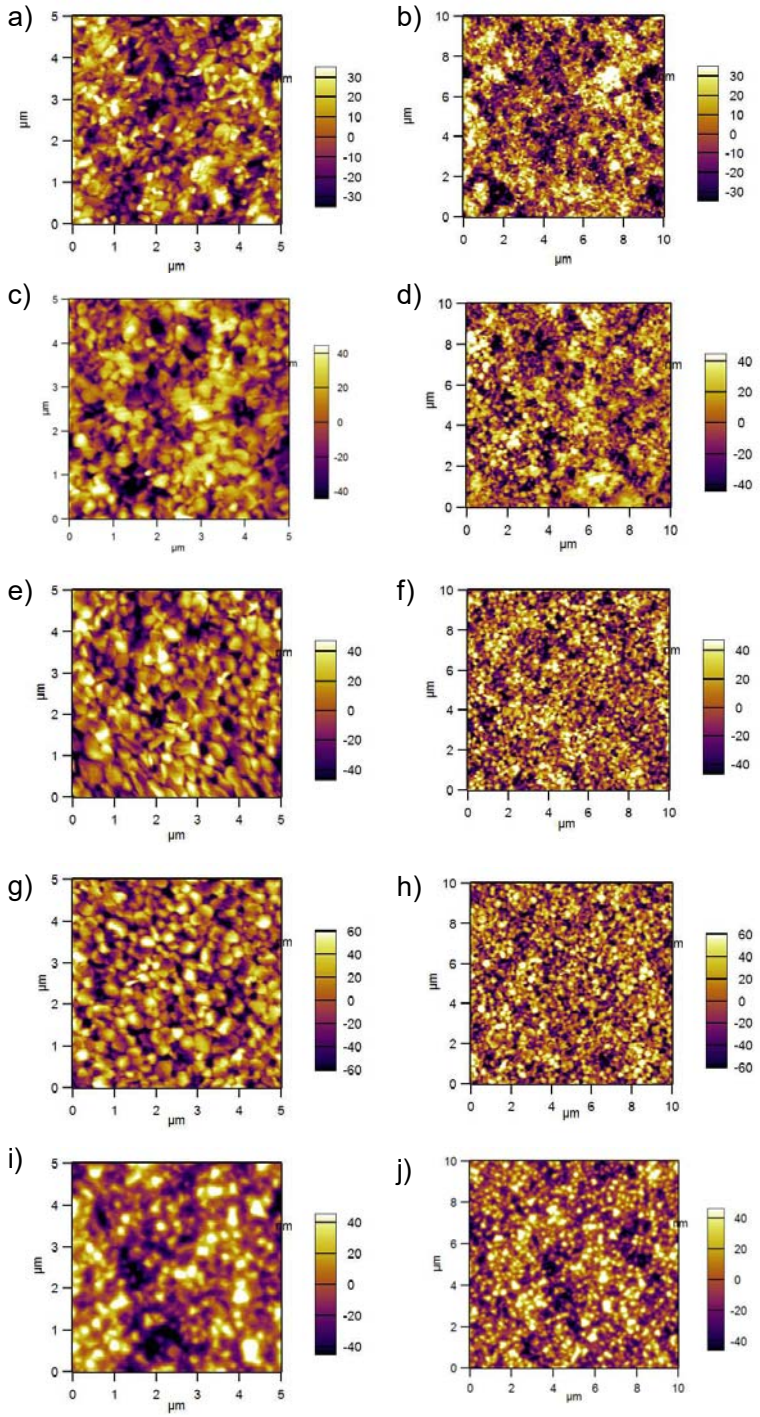

Figure S6. Topological views of perovskite films control (a and b), treated with 5mM Cs-oleate (c and d), 10mM Cs-oleate (e and f), 20mM Cs-oleate (g and h), as well as 40mM Cs-oleate (i and j), as collected from atomic force microscope (AFM). Summary of each sample's roughness is presented in Table S1.

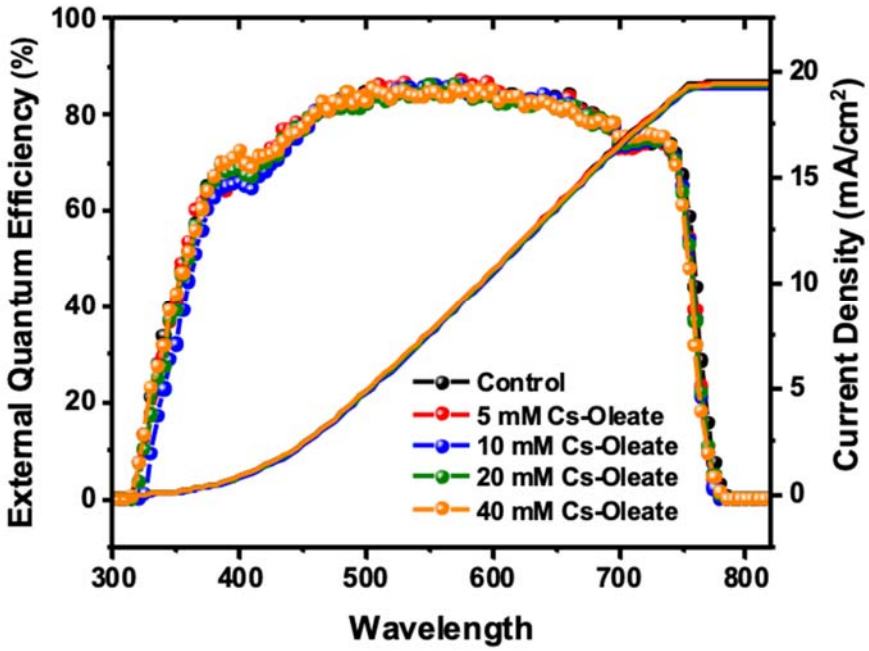

Figure S7. Incident-to-photon-conversion-efficiencies (IPCE) and integrated current density of perovskite solar cells without and with Cs-oleate treatment (1 sun; AM1.5).

Table S1. Summary of surface roughness of perovskite films with and without Cs-oleate treatment.

Sample	Area of $(5\times5)\mu m^2$	Area of $(10\times10)\mu m^2$
Control	17.669 nm	20.531 nm
5mM	21.162 nm	23.427 nm
10mM	23.631 nm	25.273 nm
20mM	30.157 nm	30.951 nm
40mM	27.000 nm	30.372 nm

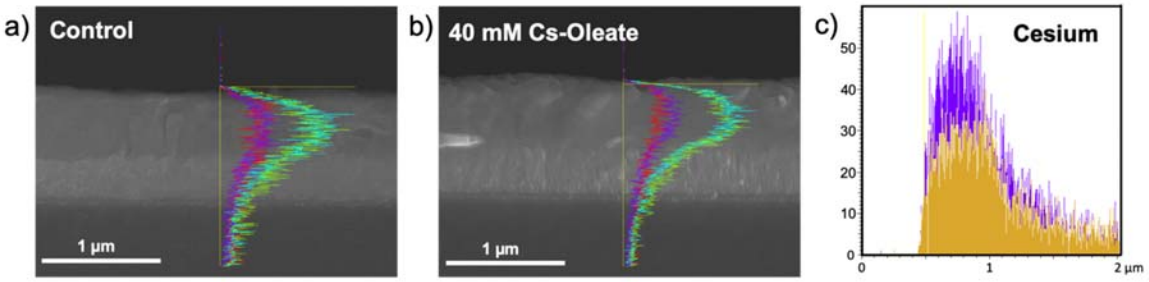

Figure S8. a) and b) Cross-sectional EDX showing the distribution of elements (cesium, lead, iodine, bromine) in control and 40 mM Cs-oleate-treated perovskite films. (Purple represents cesium La1; cyan represents lead Ma1; green represents iodine La1; red represents bromine La1) c) comparison of Cs^{+} distribution in control (yellow) and 40 mM Cs-oleate-treated (purple) perovskite films.

Samples	Band gap (eV)
Control	1.607
5 mM Cs-oleate	1.612
10 mM Cs-oleate	1.613
20 mM Cs-oleate	1.619
40 mM Cs-oleate	1.634

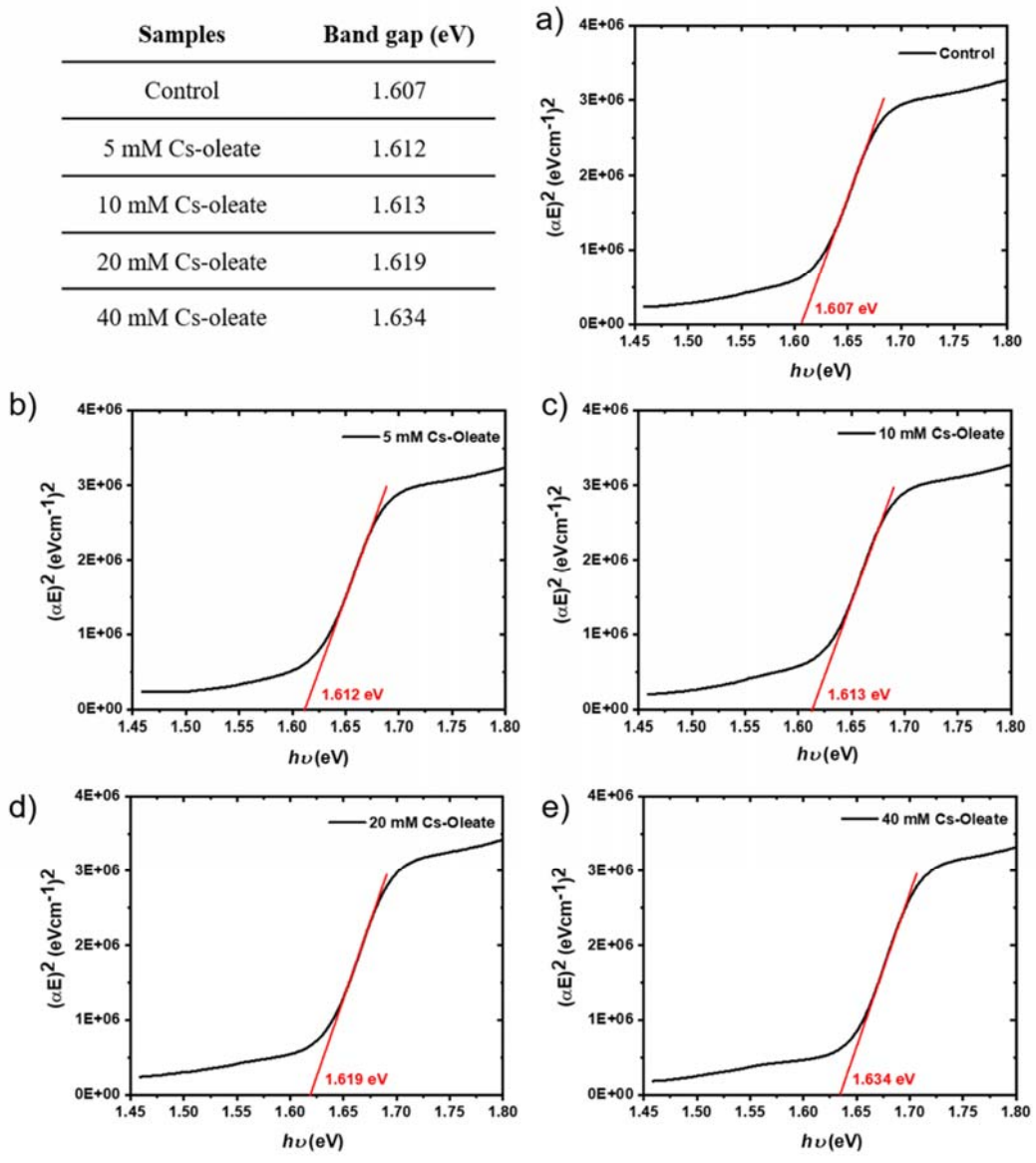

Figure S9. Bandgap and Tauc plot for control perovskite film (a) and with Cs-oleate passivation of 5 mM, 10 mM, 20 mM, and 40 mM (b-e).

Blue-shift in photoluminescence

The blue-shift of PL emission in Figure 4c is believed to be resulted from the bandgap change after Cs-oleate passivation. For 5 mM, 10 mM, 20 mM and 40 mM Cs-oleate-treated perovskite films, the bandgap is increased in the range of 0.005 to 0.027 eV, compared with control film. Therefore, it allows a blue-shift in the PL spectra.

Samples	Valence band position (eV)
Control	-5.624
5 mM Cs-oleate	-5.608
10 mM Cs-oleate	-5.568
20 mM Cs-oleate	-5.567
40 mM Cs-oleate	-5.562

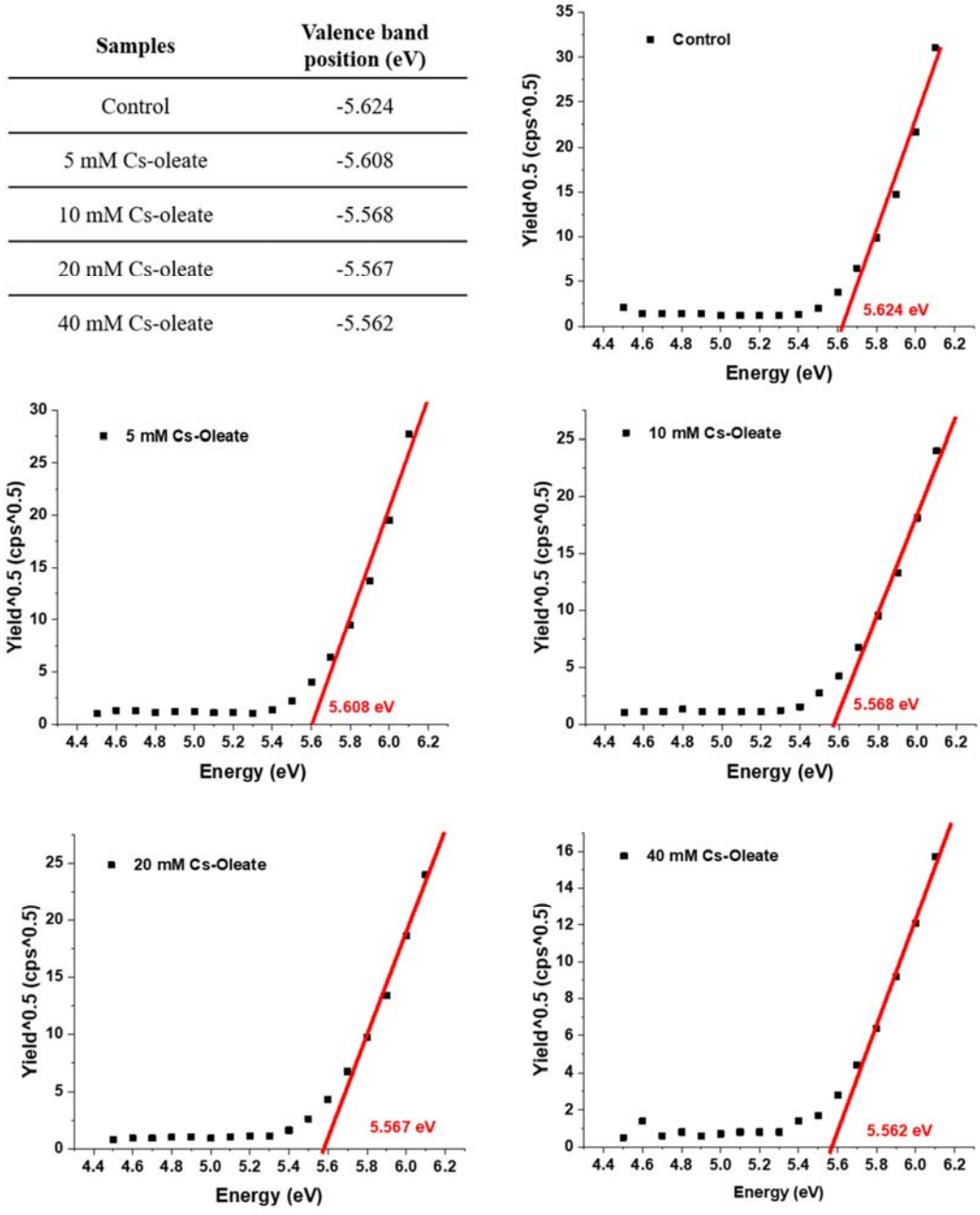

Figure S10. Valence band position of control perovskite film (a) and with Cs-oleate passivation of 5 mM, 10 mM, 20 mM, and 40 mM (b-e).

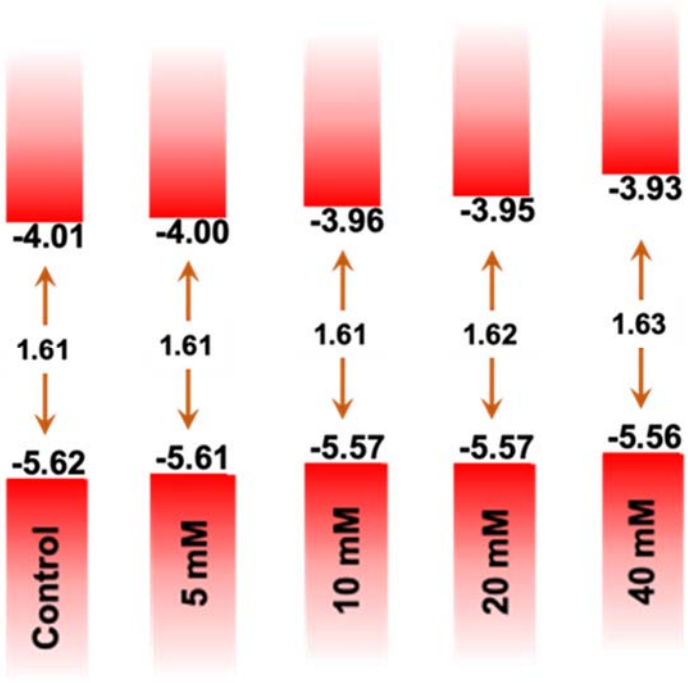

Figure S11. Energy levels of control and Cs-oleate-treated perovskite films of different concentrations.

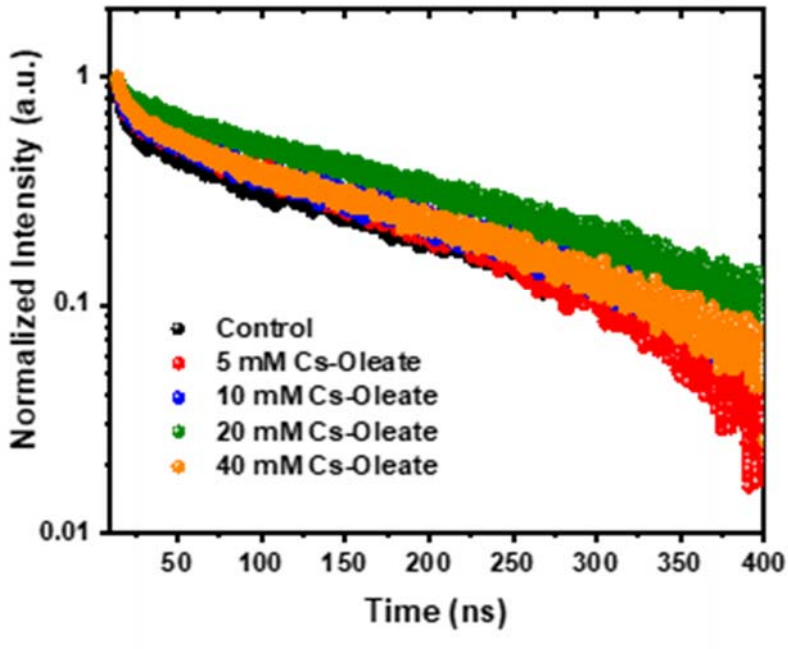

Figure S12. Time-resolved PL spectra of pristine and Cs-oleate treated perovskite films.

Table S2. Summary of photoluminescence lifetime of pristine and Cs-Oleate-treated 3D perovskites.

	τ_{ave} (ns)
Control	130.7
5mM Cs-Oleate	156.6
10mM Cs-Oleate	139.3
20mM Cs-Oleate	239.2
40mM Cs-Oleate	172.0

Table S3. The dimensions of oleate, BA and PEA.

	Oleate	**Butylammonium**	**Phenethylammo-nium**
Minimum projection area	56.87 Å^2	20.67 Å^2	24.96 Å^2
Maximum projection area	107.89 Å^2	34.40 Å^2	46.76 Å^2
Minimum projection radius	6.38 Å	2.97 Å	3.37 Å
Maximum projection radius	10.32 Å	4.58 Å	5.03 Å

Effect of Cs^+ on thermal stability

To understand the effect of Cs on stability, we synthesize MA-oleate and use it for passivation on triple cation perovskite and study the thermal stability of MA-oleate passivated film. The pristine film and 10 mM MA-oleate passivated film were annealed at 85 ℃ under inert environment for 8 hours. The XRD profile of these films are recorded and shown in Figure S13. The results show that

no significant improvement in thermal stability was observed after annealing for 8 hrs. This has highlighted the importance of Cs-rich perovskite surface for enhanced thermal stability.

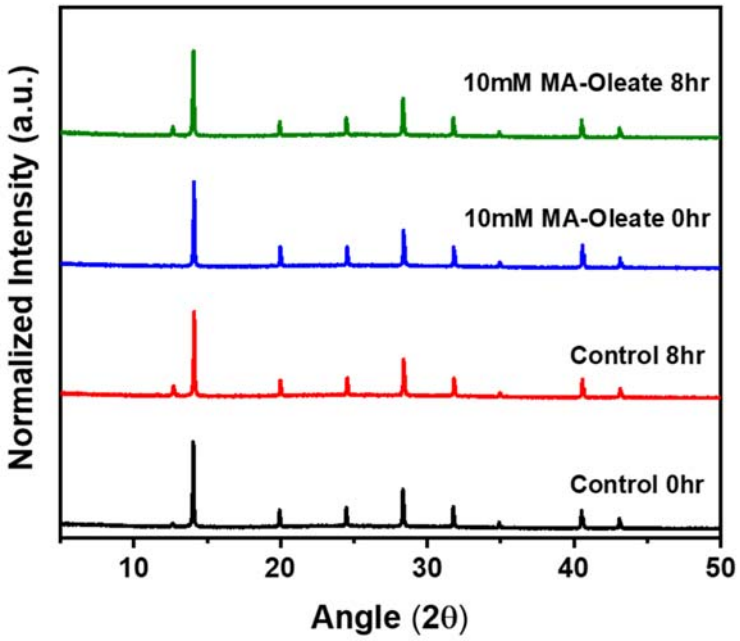

Figure S13. Thermal stability of pristine perovskite and 10 mM MA-oleate passivated films (85 ℃, 8 hr).

However, we are not able to modify the perovskite just with Cs through surface passivation, because CsI has extremely low solubility in common solvents, like toluene and isopropanol. As shown in Figure S14 below, we prepared 10 mM CsI in DMF, DMSO, toluene and IPA. It shows that CsI only dissolve in DMF and DMSO, but does not dissolve in toluene and IPA for such low concentration. However, DMF and DMSO also dissolve perovskite, so we couldn't use these solution to do surface passivation.

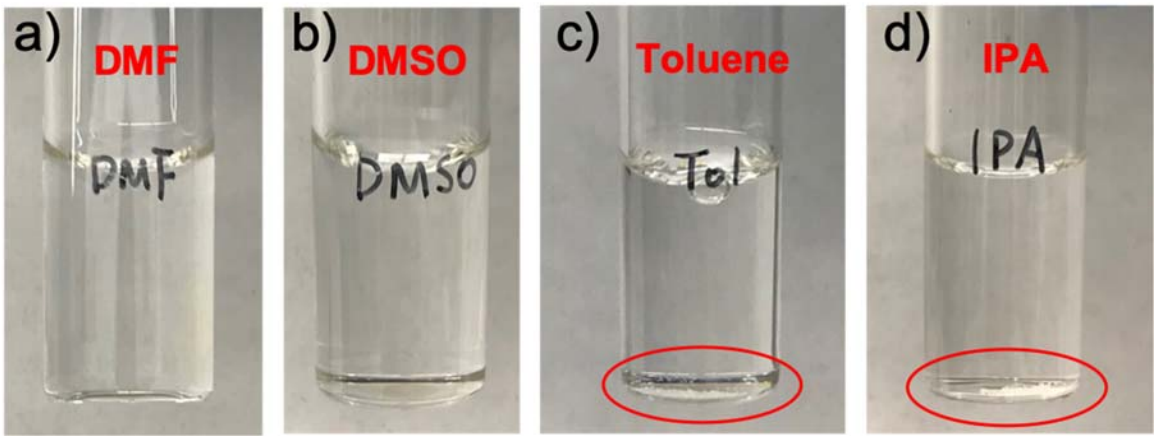

Figure S14. 10 mM CsI in a) DMF, b) DMSO, c) toluene and d) IPA solvents.

Hysteresis of IV curves

We calculate the hysteresis index based on the following equation.[1]

$$\text{hysteresis index} = \frac{J_{RS}(0.8V_{oc}) - J_{FS}(0.8V_{oc})}{J_{RS}(0.8V_{oc})}$$

The hysteresis index for the best device of control and with 10 mM Cs-oleate passivation are 0.05 and 0.11 respectively. We also calculate the average hysteresis index which are 0.11 and 0.13 for control and with 10 mM Cs-oleate passivation, respectively, which does not show significant difference.

References:

(1) Kim, H.-S.; Park, N.-G. Parameters Affecting I–V Hysteresis of CH3NH3PbI3 Perovskite Solar Cells: Effects of Perovskite Crystal Size and Mesoporous TiO2 Layer. *J. Phys. Chem. Lett.* **2014**, *5* (17), 2927–2934.